



HAL
open science

Squeal occurrence related to the tracking of the bearing surfaces on a pin-on-disc system

Van-Vuong Lai, Igor Paszkiewicz, Jean-Francois Brunel, Philippe Dufrenoy

► To cite this version:

Van-Vuong Lai, Igor Paszkiewicz, Jean-Francois Brunel, Philippe Dufrenoy. Squeal occurrence related to the tracking of the bearing surfaces on a pin-on-disc system. *Mechanical Systems and Signal Processing*, 2022, 165, 10.1016/j.ymssp.2021.108364 . hal-04508836

HAL Id: hal-04508836

<https://hal.science/hal-04508836>

Submitted on 22 Jul 2024

HAL is a multi-disciplinary open access archive for the deposit and dissemination of scientific research documents, whether they are published or not. The documents may come from teaching and research institutions in France or abroad, or from public or private research centers.

L'archive ouverte pluridisciplinaire **HAL**, est destinée au dépôt et à la diffusion de documents scientifiques de niveau recherche, publiés ou non, émanant des établissements d'enseignement et de recherche français ou étrangers, des laboratoires publics ou privés.



Distributed under a Creative Commons Attribution - NonCommercial 4.0 International License

Squeal occurrence related to the tracking of the bearing surfaces on a pin-on-disc system

Van-Vuong Lai^{a,*}, Igor Paszkiewicz^a, Jean-François Brunel^a, Philippe Dufrénoy^a

^aUniv. Lille, CNRS, Centrale Lille, UMR 9013 - LaMcube - Laboratoire de Mécanique Multiphysique Multiéchelle, F-59000, Lille, France

Abstract

Brake squeal is an important issue in the automotive and railway industry with high frequencies and acoustic pressure (above 1 kHz and 80 dB). For the comfort of passengers, the generation mechanism of this noise needs to be investigated to propose mitigation solutions. Recent works show that the state of the rubbing surface has a strong influence on the occurrences. In this paper, we propose to consider the effect of contact localization on the occurrence of squeal through experiments on a pin-on-disc system close to the braking application. An in-operando and in-situ monitoring of the contact surface during tests is carried out with thermal tracking of the friction body through thermocouples inserted in the pin near the rubbing surface. Based on the thermal measurements, an inverse method is used to identify the heat dissipation zone. Assuming that this zone is equivalent to the macroscopic load-bearing area, a stability analysis is performed to determine the unstable frequencies from contact area. Correlations between numerical results with experiments show that the change of squeal frequencies agrees with the evolution of the contact localization at a macroscopic scale. This localization can then be considered as one of the key parameters linking the surface state and the occurrence of squeal.

Keywords: Brake squeal, Contact localization, Inverse method, Stability analysis.

List of Symbols

M, C, K	Mass, damping and rigidity matrices
M_μ, C_μ, K_μ	Non-symmetrical mass, damping and rigidity matrices with the effects of the friction forces
U, \dot{U}, \ddot{U}	Vectors of nodal displacements, velocities and accelerations
λ	Complex eigenvalue
ρ	Density
c_p, k	Specific heat capacity, thermal conductivity
T	Temperature
Δt	Time step
q	Heat flux on surface $S(x_o, y_o, a, b)$
x_o, y_o, a, b	Positions and dimensions of rectangular zone
C_{ther}, K_{ther}	Capacitance and conductance matrices
E	Matrix allows to pass the local flux vector from local contact frame to global frame
T^i	Vector of nodal temperatures at step i
Q^i	Vector of local flux on the rubbing surface at step i
E	Observation matrix in which the position of the measured points in global vector is determined
Y^i	Vector of numerical temperatures at step i
Y_{mes}^i	Vector of measured temperatures at step i
g_T	Relative gap between the numerical and measured temperature

1. Introduction

A braking system is a vital component that helps to ensure the safe operation of vehicles. Among the different braking technologies used in transport, braking by friction is still the most commonly used, particularly in cases of

*Corresponding author

Email address: vanvuong.lai1990@gmail.com (Van-Vuong Lai)

5 emergency. The kinetic energy of the vehicle is transformed into other energies, mainly heat, when the brake pads rub against the brake disc. Related to the use of friction brakes, several problems (for instance: thermal fatigue [1], friction instabilities [2], wear [3, 4], particle emission [5], and noise emissions like squeal [6, 7]. . .), have still been significant challenges for the automobile industry. Brake squeal is a relevant issue for the automotive and rail industries because of its frequency range contents (from 1 to 16 kHz) and noise levels up to 100 dB. The research community commonly
10 accepts that this noise results from self-excited vibrations of the brake system due to its unstable dynamical behavior under sliding frictional contact conditions [8–10]. Despite the many works in the domain of friction-induced vibration that are experimental, numerical, or analytical, the conditions responsible for brake squeal are still controversial. Firstly, in terms of instability mechanisms, brake squeal can be mathematically triggered by mode-coupling [10] even with a constant friction coefficient or by the falling friction coefficient with relative sliding speed [11, 12]. Secondly,
15 brake squeal depends sensibly on several factors at multi-scales: behavior of structural components (geometry of the components or connections between components [13], material properties [14], thermal effect [15, 16]), external excitations (applied pressure [17], humidity [18]) as well as behavior of the friction interface during braking.

For two decades, by several experiments and numerical works, many researchers have conducted investigations on the behavior of the brake interface for a better understanding of the generation mechanism of brake squeal. They
20 showed the dependency of the mechanical system dynamical behavior on the brake interface behavior at both micro and macro scales. At a macroscopic scale, the dependency of pad geometry has been studied [19], and chamfering the brake pin or adding slots are solutions currently used to reduce squeal occurrence. By a simplified "pin-on-disc" system, Duboc *et al.* [20] obtained different squeal frequencies with different pin geometries. Xiang *et al.* [21] found that the friction block shape has a significant effect on the contact pressure distribution. The hexagonal friction block
25 exhibits a more uniform distribution of contact pressure than the pentagonal and circular friction blocks, resulting in the lowest contact stiffness as well as the slightest noise. At a smaller scale (micro-scale), the evolution of contact surface heterogeneity (due to material degradations and apparition of the third body) has a strong influence on squeal [22]. This evolution is linked with the tribological circuit and the friction material, which is considered heterogeneous and with a complex behavior [23]. The effect of wear on the occurrence of squeal in the braking system was reported
30 in [6, 24]. Some researchers have shown that due to the tribological circuit, contact plateaus including wear debris accumulated and compacted around primary plateaus on the pad are formed [25]. During the circuit, plateaus can also disintegrate and be removed progressively. This contact time–space evolution has been illustrated in [26, 27]. By an experimental study along with numerical simulation of the sliding interface, Lee *et al.* [28] explained that the size of the contact plateau distribution has a strong impact on the stick–slip amplitude and oscillation frequencies of brake
35 friction materials. Using a simplified customized test rig with a transparent glass disc and an artificial alumina third-body, Singla *et al.* [29] observed that the occurrence of squeal is apparently linked to the change in the redistribution of thirdbody particles in the interface, which strongly influences the location of the load-bearing area. Xiang *et al.* [30] indicated that at different brake disc rotation speeds, vibration responses and contact behaviors evolve. The strongest vibration response occurred at a low brake disc rotation speed (200 rpm). At this speed, the friction block
40 exhibited higher friction and severe localized wear, and a rough wear surface. In parallel with these phenomenological observations, several numerical works have tried to quantify the influence of contact surface heterogeneity (in terms of profilometry or local mechanical properties) [31–33] on squeal occurrence. The quantitative properties may be added in numerical modeling at a macroscopic scale. Tison *et al.* [33] showed that the perfectly flat and homogeneous contact state may under or over-estimate the unstable frequencies and numerical simulations need to take into account contact
45 surface heterogeneity. With the same pin geometry, the contact distribution evolves due to the thermal dilatation as reported in [34]. Numerical results, obtained by the authors [35], exhibited that with a pin–on–disc geometry, there is a strong correlation between contact localization and the occurrence of squeal frequencies at the macroscopic scale. They showed that by varying the location and dimensions of the effective contact zone, two different squeal frequencies can be found.

50 These rather experimental observations and numerical simulations naturally lead to the question of the time–space evolution of contact state during braking and its implication on the occurrence of squeal. However, the contact state can only be measured and characterized before and after friction applications (post-mortem). The contact time–space evolution is unknown during sliding since the contact zone is inaccessible. Thus, it is proposed in this work to investigate rubbing contact area variations during tests and their influences on the occurrence of squeal with a dynamic
55 tracking of the load-bearing area using a map of thermal measurements. The steps-wise procedure followed for carrying out the analysis is shown in Fig. 1. Firstly, squeal tests are developed on a pin–on–disc system that is simpler than a braking system from a dynamic point of view: fewer modes, easier modal identification, and lower nonlinearities due to connections. Monitoring of the contact surface is carried out with thermal tracking of the friction body through thermocouples and using an inverse method to determine the heat flux distribution and area at the contact surface.
60 Assuming that the heating area corresponds to the rubbing one, this area is used for the stability analysis done with complex eigenvalue analysis. At the same time, squeal frequencies are detected from noise measured by a microphone, and correlation between unstable modes from the stability analysis and the occurrence of squeal can be done.

The main originality of this work is to be able to track dynamically the load bearing-area during the tests and

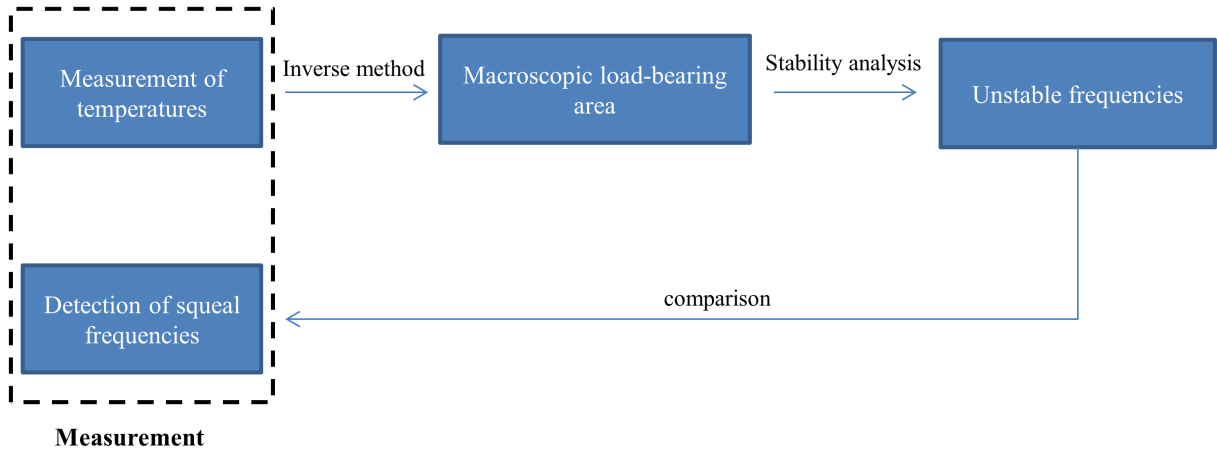


Figure 1: Steps-wise procedure followed for carrying out the analysis

corresponding instabilities thanks to a map of thermocouples and inverse method.

This paper is divided into two parts: the first one (Section 2) details the experimental means and data treatment to determine the effective contact area variations, and the second part (Section 3) is devoted to the results for a series of test and comparison between squeal detection and unstable modes from the stability analysis.

2. Experimental means and multi-modal data treatment for identification of the load-bearing area

2.1. Experimental set-up

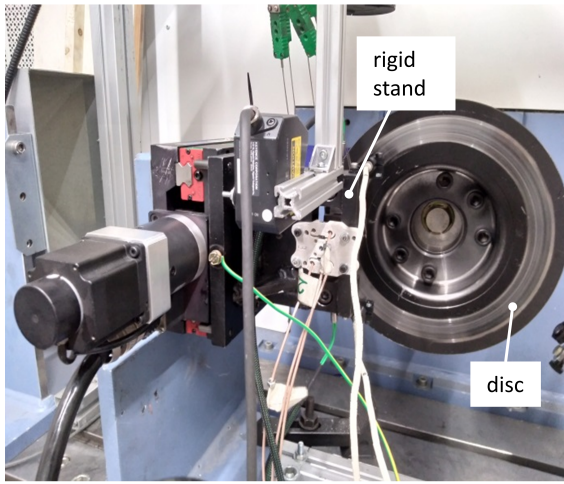
According to the objectives, squeal tests are performed on the set-up developed in [20] that allows for the study of the role of the interface behavior on squeal generation. Fig. 2 shows the experimental set-up based on a pin-on-disc configuration. It is made of a rigid stand on which a blade is attached to its extremities. The pin is glued at the center of the blade. The displacement along the axial disc direction pushes the pin against the disc, and the bending of the blade gives the normal load. To increase the tests reproducibility and facilitate the correlation with modeling, the architecture limits the connections between the components. The disc is made of 15CrMoV6 steel. The average diameter of the sliding track is 100 mm. The pin is made of a sintered composite material with a metal matrix (copper and iron) and graphite particles. The sliding contact area is a 20 mm x 20 mm square face.

The experimental frequencies of the disc and the pin have been determined without disc-pin contact using impact hammer and acceleration measurements. For the disc, out-of-plane impact and out-of-plane acceleration measurements are carried out. Fig. 3 shows the frequency response function FRF for the disc and pin. Tab. 1 shows the eigenfrequencies of the disc in comparison with those obtained from FE model in [35]. These FE modes are classified according to predominant movement, number of nodal circles and number of nodal diameters. The peaks of this frequency response function correspond to axial modes with no nodal circles. The differences between these measured frequencies and these FE frequencies are less than 4.5%.

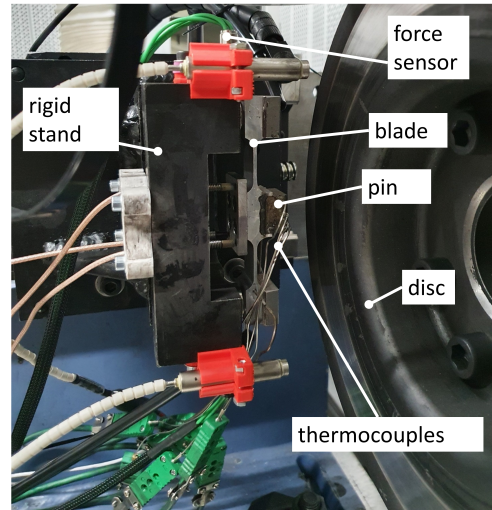
Measured frequencies (Hz)	FE frequencies (Hz)	Mode type (a,m,n)
852	892	(a,0,0)
1278	1261	(a,0,2)
2250	2220	(a,0,3)
3725	3694	(a,0,4)
5614	5571	(a,0,5)
7821	7776	(a,0,6)

Table 1: Eigenfrequencies of the disc (a: axial predominant movement, m: nodal circles and n: nodal diameters) [35]

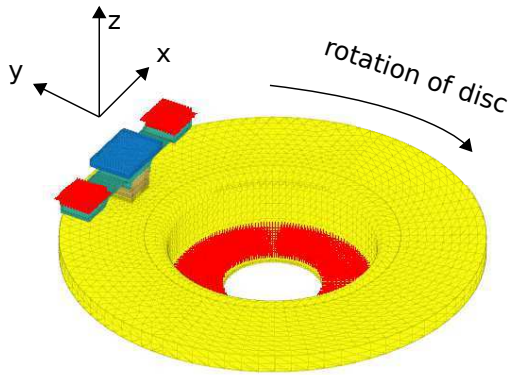
For the group, including the pin together with plates attached on a rigid stand, which is called "pin" for the following sections, impact and acceleration measurements have been performed at different positions to identify its eigenfrequencies. Tab. 2 shows the three first eigenfrequencies of the pin without contact with the disc. These frequencies correspond to the three biggest magnitudes of the function FRF. The differences between these measured frequencies and these FE frequencies are inferior to 7%. The modes shapes are presented in Fig. 4 and can be found in [35]. These modes represent vertical translation (second mode) and rotational movements (first and third modes) of the pin. Reportedly, these three first modes contribute principally in modes coupling [20]. For the higher eigenfrequencies, FRF value is greatly smaller than for the three first frequencies.



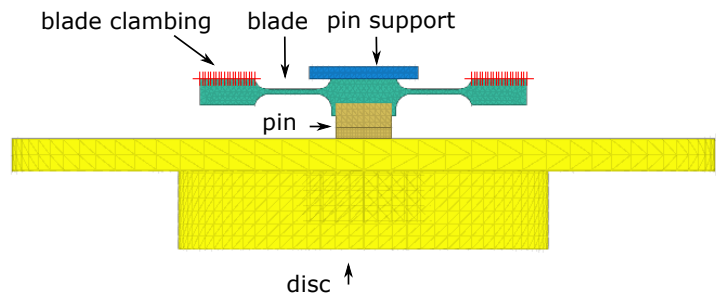
(a) experimental device



(b) zoom near contact zone

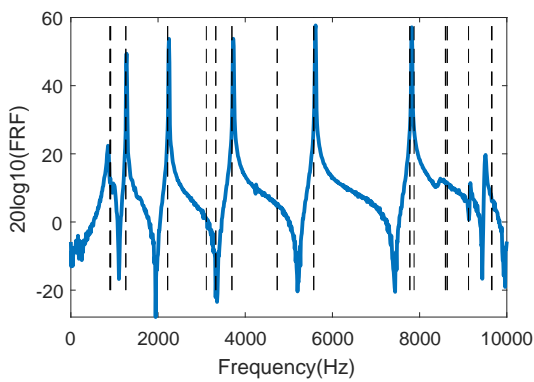


(c) 3D

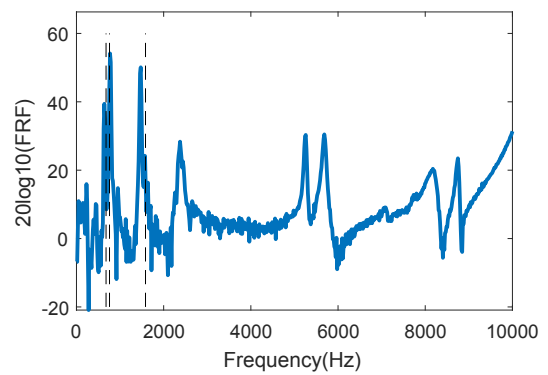


(d) 2D

Figure 2: Experimental set-up of the pin-on-disc system (a,b) [20] and corresponding FEM model (c,d) [35] used for stability analysis



(a) Disc



(b) Pin

Figure 3: Frequency response function of the disc and the pin impacted by hammer (dotted lines: FE eigenfrequencies)

Measured frequencies (Hz)	FE frequencies (Hz)
639	678
770	758
1475	1584

Table 2: Eigenfrequencies of the pin [35]

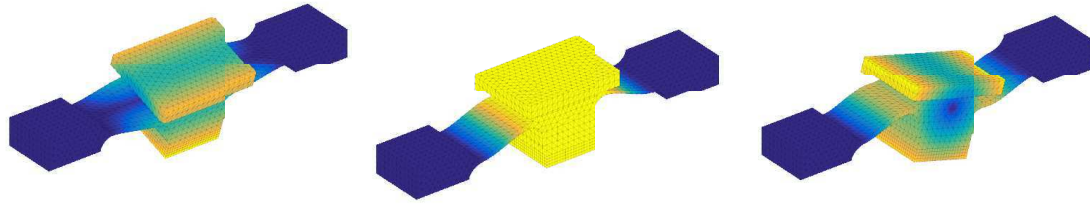


Figure 4: Three first mode shapes of the pin [35]

2.2. Tests procedure and measurements

Based on this experimental set-up, friction tests are performed. The complete test sequence is divided into test series of 10 successive friction tests, including contact and no-contact conditions (30s for each). A timeline of the protocol is shown in Fig. 5. For each test, the rotation speed remains constant. The change of rotation speed from 200 rpm to 500 rpm aims to act on contact localization, which is subsequently analyzed. Several measurements are performed along the test sequence:

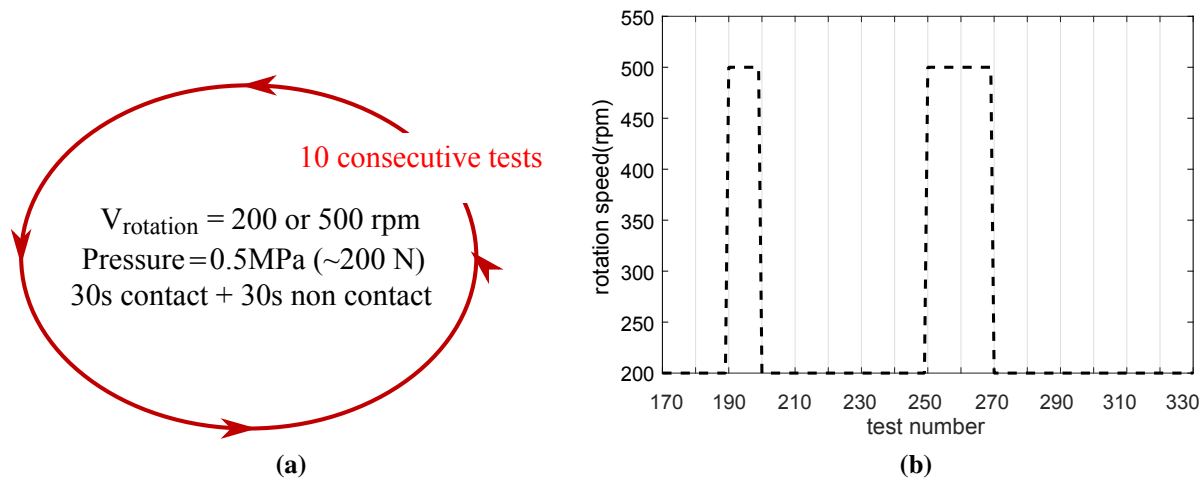


Figure 5: Protocol for friction test series (a) and variation of rotation speed during series (b)

- Acoustic measurement for the determination of the noise occurrence and associated frequencies.
- Thermal measurements of the pin to identify at a macroscopic scale the load bearing area.
- Apparent friction coefficient is computed as a ratio between measured tangential force and normal forces. The resulting contact forces are measured using piezoelectric sensors at the extremities of the blade (Fig. 2b).

The following parts present more in details the technical acoustic and thermal measurements as well as the associated treatment of the data.

2.2.1. Acoustic measurement

During sliding, the sound is recorded at 50 kHz leading to noisy frequencies analysis up to 25 kHz. The microphone is located at a distance of 1m from the disc-pin contact plane. Two treatments are proceeded. First, a short-time Fourier Transform giving information about the transient evolution of the noise frequencies (presence of harmonics, duration of the noise events) is used. Generally, brake squeal is defined as a tonal sound in the audible frequency range above 1 kHz at perceivable amplitude. The tonal character restricts the vibration energy to being confined to a narrow frequency range, i.e. a sharp dominant and weakly damped peak in the signals Fourier transform. The second treatment is about the squeal frequencies detection. Using Fourier transform with a sliding window approach, amplitude spectra are computed for successive instants of the vibration measurement. Peaks are identified in the spectrum. As squeal frequencies may shift slightly over time, peaks are assigned to a single group if they do not differ by more than a specific frequency gap, e.g. 200 Hz. For each frequency group, the duration of a tonal sound event above the critical sound pressure level (80 dB), is evaluated. This approach, which depends on the chosen pressure level, may underestimate squeal frequencies [36]. Thus, it is necessary to re-verify identified squeal frequencies by

listening to each audio. Fig. 6 shows the spectrogram of the sound measured by a micro and the temporal evolution of squeal frequencies for test 180. For this test, the detected frequencies are 3637Hz and 5440Hz, respectively.

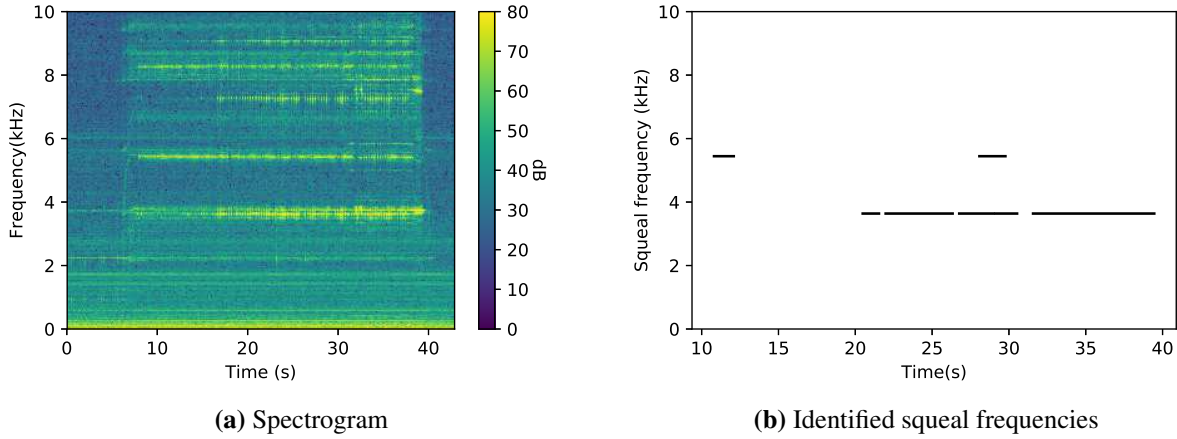


Figure 6: Spectrogram of the sound measured by a micro (a) and identified squeal frequencies (b) for test 180. Reference velocity: 2×10^{-5} m/s.

120 2.2.2. Thermal measurements

The thermal instrumentation of the pin is composed of 8 thermocouples inside the pin at average 3 mm depth from the contact surface. Obviously, the more thermocouples are installed inside the pin, the better the quality of monitoring of the contact surface is. However, the drilling of the pin for too many thermocouples can disrupt the thermal and dynamic properties of the pin. Thermal paste with high thermal conductive is used to fix the thermocouples during tests. As mentioned earlier, the position of thermocouples is important for the inverse method. Thus, this is precisely localized using X-ray tomography via ISIS4D platform. The positions of the thermocouples are plotted in Fig. 7. The z- position of thermocouples varies by about 1mm. The sampling frequency for the thermal measurement is 100 Hz.

2.3. Identification of the load-bearing area from thermal measurements

In order to localize the contact zone, three methods can be used: ultrasonic method [37], pressure-sensitive films [30, 38] and inverse thermal method [39]. These first two methods remain limited to static analyzes. On the other hand, the inverse heat flux method consists of determining the heat flux distribution, which minimizes the difference between the computed temperatures compared to the experimental ones. This method is then able to monitor the dynamical evolution of the contact zone during the test. A large number of analytical and numerical techniques have been developed for the solution of the inverse heat conduction problems, for instance, iterative gradient methods [40–42], sequential function specification techniques [43, 44], stochastic optimization techniques [45], Monte Carlo methods [46, 47], methods comprising filtering techniques [48], and neural networks [49–51]. These models are still used for one-dimensional analytical problems. In addition, the number of measured points has often been inferior to that of estimated flux. The inverse problems then become ill-posed due to this lack of continuity of the solution to the experimentally measured data.

From the previous thermal measurements, an inverse thermal method is proposed to estimate the load-bearing area, which corresponds to the area where the mechanical power is dissipated. The aim is to determine heat flux distribution that corresponds to the evolution of measured temperatures. Being fixed, the pin is not sensitive to the convective heat dissipation effect with the air environment during contact. Thus, the convective heat dissipation is neglected for the pin. Tests are performed with a relatively low energy level, with the increase of temperature $< 150^\circ\text{C}$. For the chosen friction material (sintered material), by thermal properties measurements using Laser Flash Analyser, thermal properties are independent of temperature. The thermal behaviors of the disc, the blade and the pin support are isotropic while the thermal behavior of the pin is transversal isotropic. The thermal data is given in Tab. 3. In this study, the frictional heat is assumed only generated by the frictional contact force at the contact area.

Considering a system (domain Ω) where heat transfer is performed by diffusion and exchange with air and all initial conditions are supposedly known, the mathematic equation describing heat transfer is given by the energy balance obtained from the first law of thermodynamics and Fourier's law of heat conduction:

$$\rho c_p \frac{\partial T}{\partial t} = k \Delta_{x,y} T, t > 0 \quad (1)$$

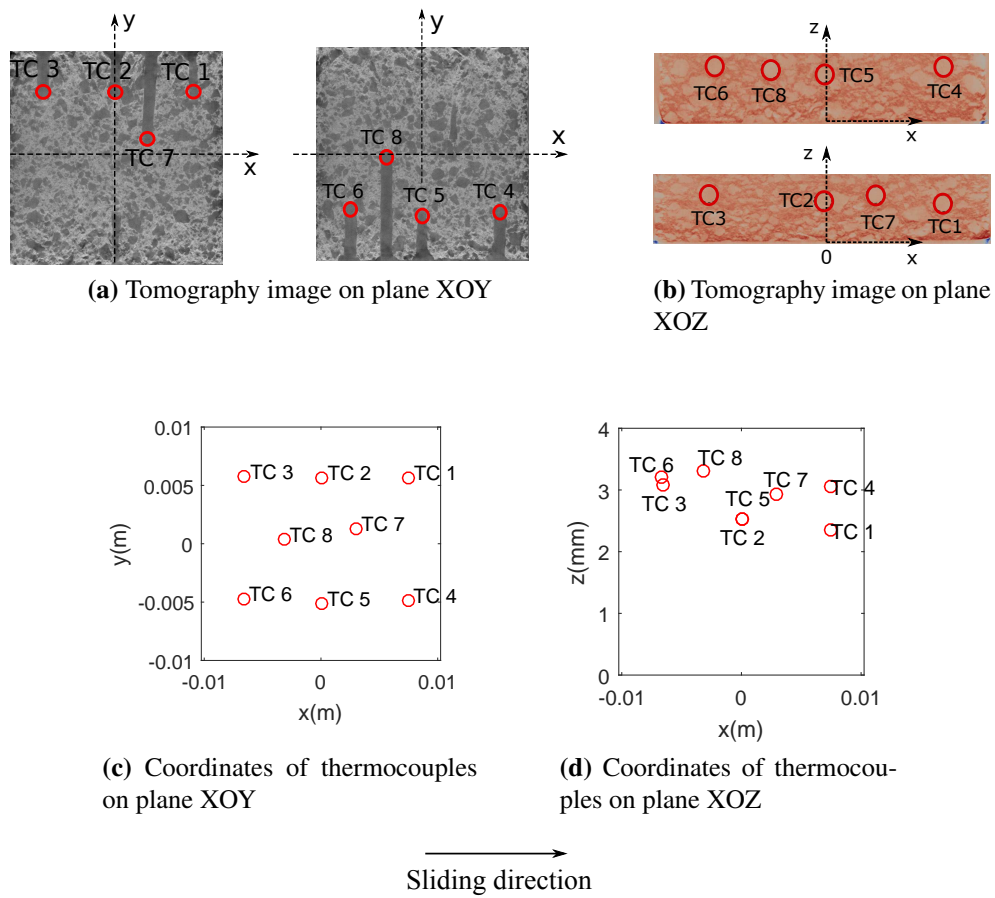


Figure 7: Position of thermocouples inside the pin localized by X-ray tomography (a,b) and identified coordinates of thermocouples on planes XOY and XOZ (c,d). The x - axis relates to the length of the pin (20 mm) along the tangential sliding direction and y - axis relates to the length of the pin along the disc radius.

Data	Disc	Pad	Thin plate	Thick plate
Thermal conductivity k ($\text{Wm}^{-1}\text{K}^{-1}$)	50	$k_x = k_y = 45, k_z = 20$	200	30
Heat capacity c ($\text{JK}^{-1}\text{kg}^{-1}$)	450	400	900	400

Table 3: Thermal data

where ρ is the density, c_p is the specific heat capacity, and k is the thermal conductivity, and T is the temperature.

As mentioned above, in this case where the number of measured points (8 points) is inferior to that of estimated flux (462 points), the inverse problem is ill-posed, making the solution very sensible with error and non-uniqueness. That is why in this study, to obtain a more stable solution, more information should be added leading to some following assumptions. We assume that the estimated flux is positive and uniform at a rectangular zone, as shown in Fig. 8. This rectangular zone $S(x_o, y_o, a, b)$ is characterized by dimensions (a, b) and location (x_o, y_o) . With these assumptions, the load-bearing area can be identified only at the macroscopic scale. It must be noted that only the dimensions (a, b) superior to 7 mm can be identified, taking into account the distance between thermocouples of about 7 mm.

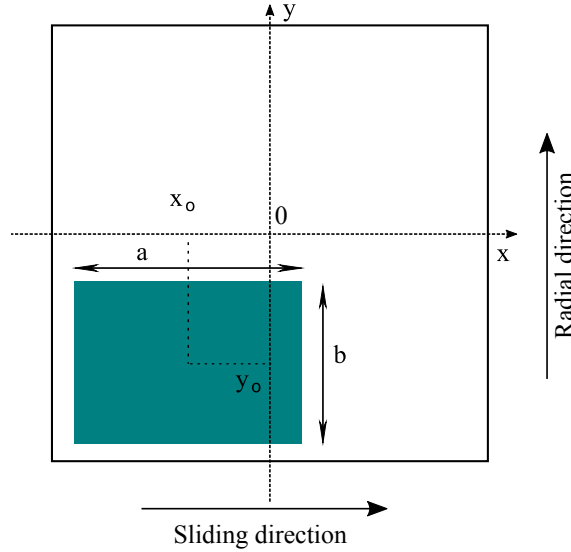


Figure 8: Scheme of the macroscopic contact area with parameters (position (x_o, y_o) , dimensions (a, b) , radial direction from inner radius to outer radius)

The solution to this problem is subject to the following boundary and initial conditions:

$$k \nabla T \cdot n = q \quad \text{on } S(x_o, y_o, a, b) \quad (2)$$

$$T = T_o \quad \text{if } t = 0 \quad (3)$$

where q is normal heat flux on $S(x_o, y_o, a, b)$ with normal direction n . This flux is a result of friction heat flux.

FEM form of these above equations Eqs. (1) to (3) at the current time step i using the variational principle and Euler backward time difference method [52] is given as:

$$(\mathbf{C}_{ther} + \Delta t \mathbf{K}_{ther}) \mathbf{T}^i = \mathbf{C}_{ther} \mathbf{T}^{i-1} + \Delta t \mathbf{E} \mathbf{Q}^i \quad (4)$$

where the capacitance matrix \mathbf{C}_{ther} , the conductance matrix \mathbf{K}_{ther} and the flux vector \mathbf{Q}^i at step i . Matrix \mathbf{E} allows to pass the local flux vector from local contact frame to global frame. The detail of these matrices can be found in [53].

The temperature at step i is deduced from Eq. (4):

$$\mathbf{T}^i = \mathbf{D} \mathbf{T}^{i-1} + \mathbf{F} \mathbf{Q}^i \quad (5)$$

where $\mathbf{D} = (\mathbf{C}_{ther} + \Delta t \mathbf{K}_{ther})^{-1} \mathbf{C}_{ther}$ and $\mathbf{F} = (\mathbf{C}_{ther} + \Delta t \mathbf{K}_{ther})^{-1} \mathbf{E}$.

The temperatures at measured points at step i are obtained through observation matrix \mathbf{H} in which the position of the measured points in global vector is determined:

$$\mathbf{Y}^i = \mathbf{H} \mathbf{T}^i \quad (6)$$

Substituting Eq. (5) in Eq. (6), we have:

$$\mathbf{Y}^i = \mathbf{H} \mathbf{D} \mathbf{T}^{i-1} + \mathbf{H} \mathbf{F} \mathbf{Q}^i \quad (7)$$

Finally, the estimated flux \mathbf{Q}^i has to verify Eq. (7). Thus, basing on this equation, the problem is to find uniform distribution flux on a zone with dimensions (a, b) and location (x_o, y_o) which minimizes the difference between measured \mathbf{Y}_{mes} and numerical temperatures \mathbf{Y}^i . It then becomes a minimization under constraints:

$$\mathbf{Q} = \underset{\mathbf{Q}^i > 0}{\operatorname{argmin}} g_T \quad \text{on } S(x_o, y_o, a, b) \quad (8)$$

where

$$g_T = \frac{|\mathbf{HFQ}^i + \mathbf{HDT}^{i-1} - \mathbf{Y}_{\text{mes}}^i|}{|\mathbf{Y}_{\text{mes}}^i|}$$

170 g_T is the relative gap between the numerical and measured temperatures. $|\bullet|$ denotes the norm of vector \bullet . The resolution of Eq. (8) is carried out by using the conjugate gradient method available in Matlab. For each (x_o, y_o, a, b) , the process is repeated up to minimizing the gap between the computed temperatures compared to the experimental ones g_T . The solution gives the location and dimensions of approximated contact zone as well as uniform contact flux intensity. With the size mesh of 1mm, there are about 3700 candidates $S(x_o, y_o, a, b)$, meaning that about 3700 possible
175 contact zones need to be tested to find an optimal one. As in [53], the flux may be assumed constant on $1 \Delta t$ or $N\Delta t$.

Fig. 7a shows the measured temperatures against time at the eight positions of thermocouples for a friction test of 30s. The normal force is around 200N and the disc rotation is 200 rpm. Results are plotted in terms of the increase of temperature during the test (i.e., gap with the initial temperature) and not in absolute temperature. It can notice that temperatures are not the same for all thermocouples, mainly due to a non-uniform disc-pin heating zone. This
180 inverse method, based on Eqs. (1) to (8), is applied to determine this heating zone. Firstly, it is assumed that the heat flux distribution is constant during the whole test. Fig. 7b shows the numerical temperatures at the 8 positions of the thermocouples for the optimal solution. The optimal solution is chosen as the criterion $\min g_T$ is satisfied. The global trend (in terms of transient evolution and final temperature) is reproduced. Even if the order of thermocouples is not exactly the same, it can be observed that the temperatures for thermocouples 4, 5, 6, 7 and 8 are higher than those for thermocouples 1, 2, 3. Physically it can be interpreted as a heating zone mainly around the inner and the mean radius. Fig. 7c shows the difference 180 between the measured and numerical temperatures. In the beginning, this difference is large (about 3 °C) however it then decreases (about 1 °C).

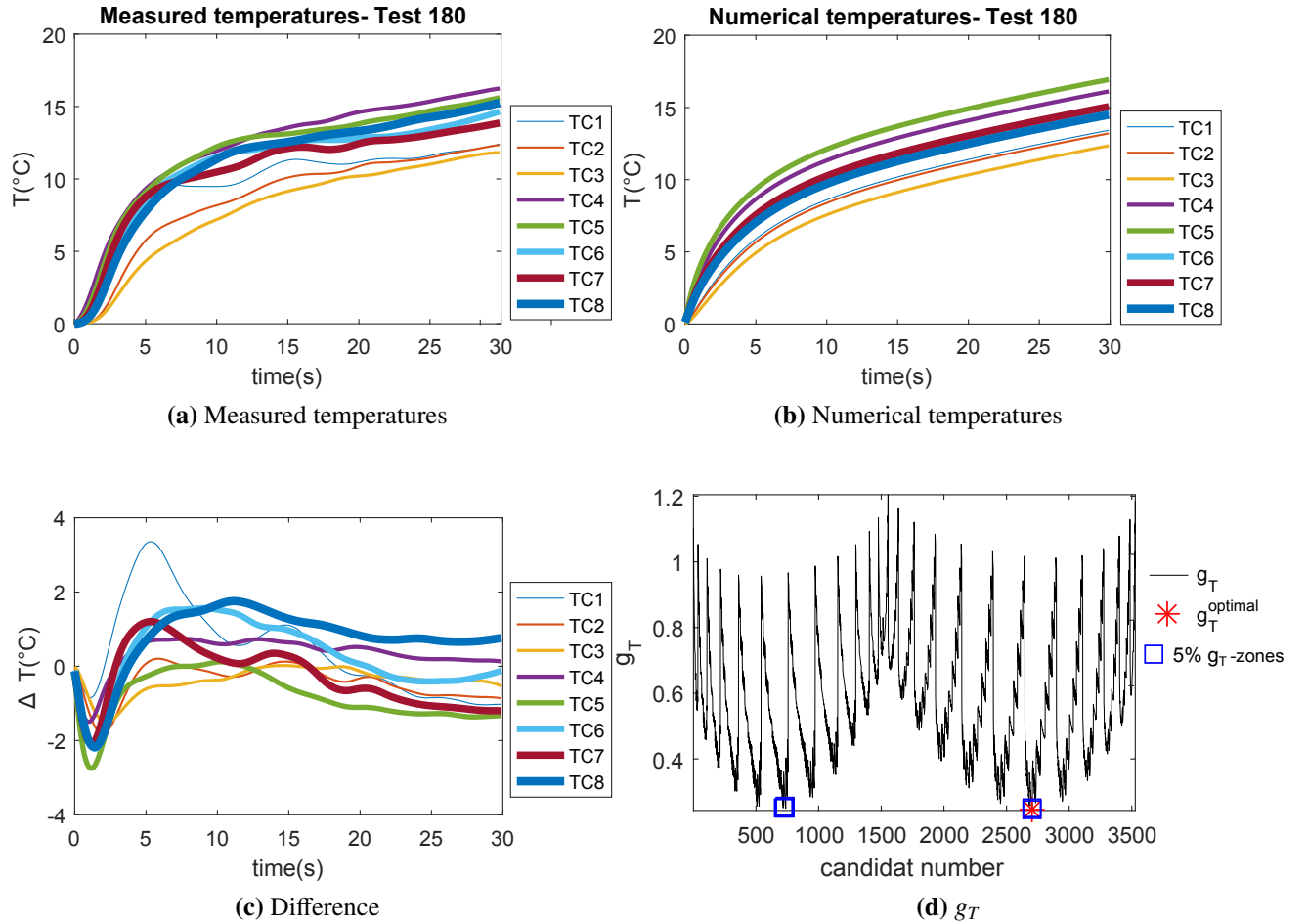


Figure 9: Results obtained by inverse method by assuming that the flux distribution is constant during the whole test (a: measured temperatures, b: numerical temperatures, c: difference between measured and numerical temperatures, d: relative gap between the numerical and measured temperature)

Fig. 9d also shows the value of g_T for all candidates $S(x_o, y_o, a, b)$. There are some potential solutions that give g_T close to the optimal one (difference inferior 5% on g_T in Eq. (8)). The corresponding identified contact zones

190 are presented in Fig. 10. To facilitate the lecture, these zones are called "5%g_T- zones" for the following sections. Together with the optimal zone, they cover mostly the position of thermocouples 4, 5, 6, 7 and 8. That is why the temperatures in these thermocouples are higher than those in thermocouples 1, 2, 3. The maximal difference between the optimal and close zones is about 2mm on dimensions. This means that there is a sensibility on the identification of the contact zone. Thus, the sensibility is taken into account for the following stability analysis.

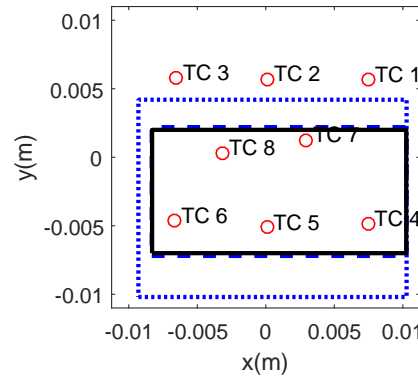


Figure 10: Optimal identified contact zone (black solid line) and 5%g_T- zones situated between two blue rectangles.

195 To follow the temporal evolution of flux distribution, by using the same inverse method but assuming that the flux distribution can vary every second, Fig. 11a shows the numerical temperatures against time at the 8 positions of the thermocouples. The temporal evolution of numerical temperatures is a little bit closer to the experimental ones (Fig. 9a). As presented in Fig. 11b, the difference between measured and numerical temperatures is smaller (< 2°C) for thermocouple 1, compared to the case of flux constant during the whole test. Fig. 12 shows the temporal evolution of identified parameters (x_o, y_o, a, b) in comparison with the identified ones in the case of constant heat flux distribution during the whole test. In the beginning (before 5s), these values are highly different from the identified ones in the case of constant heat flux distribution during the whole test. It can be explained by the fact that the loading is progressive until the contact zone is stabilized. After 5s, this difference decreases (about 1 mm). It can be explained by the fact that the loading is progressive until the contact zone is stabilized. That is the reason why for the following section, results obtained with a constant heat flux over the tests are presented.

200

205

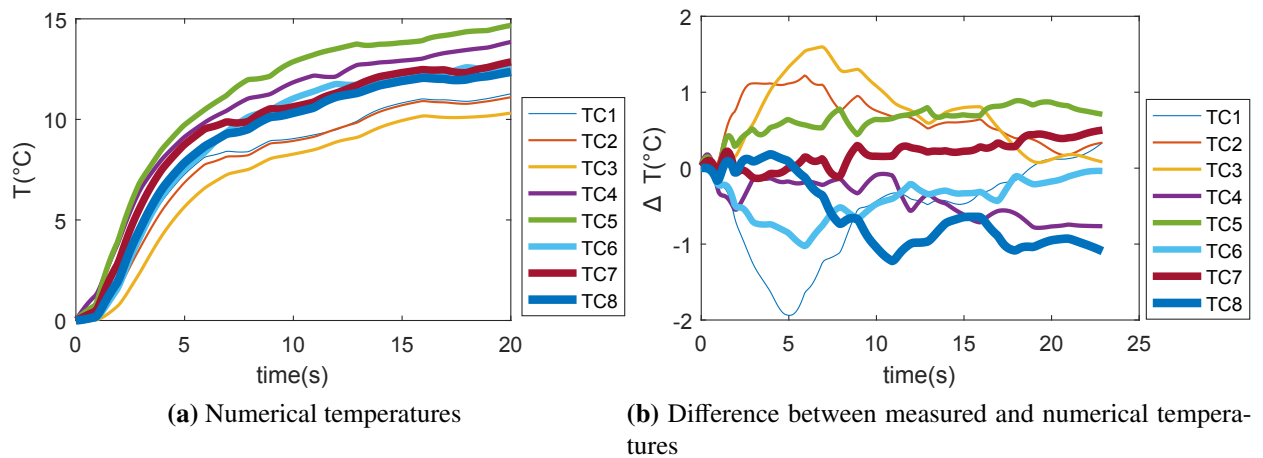


Figure 11: Numerical temperatures (a) and difference between measured and numerical temperatures (b) in the case of flux distribution constant for each second

In this section, an inverse thermal method that allows for the localization of the load-bearing area is developed and applied to a test. With this method, one can approximate the location and dimensions of load-bearing area at the macroscopic scale using the assumption of constant heat flux during the test. In the following subsection, a numerical model for stability analysis of the mechanical system, which can take into account the evolution of load-bearing area during tests, is presented.

210

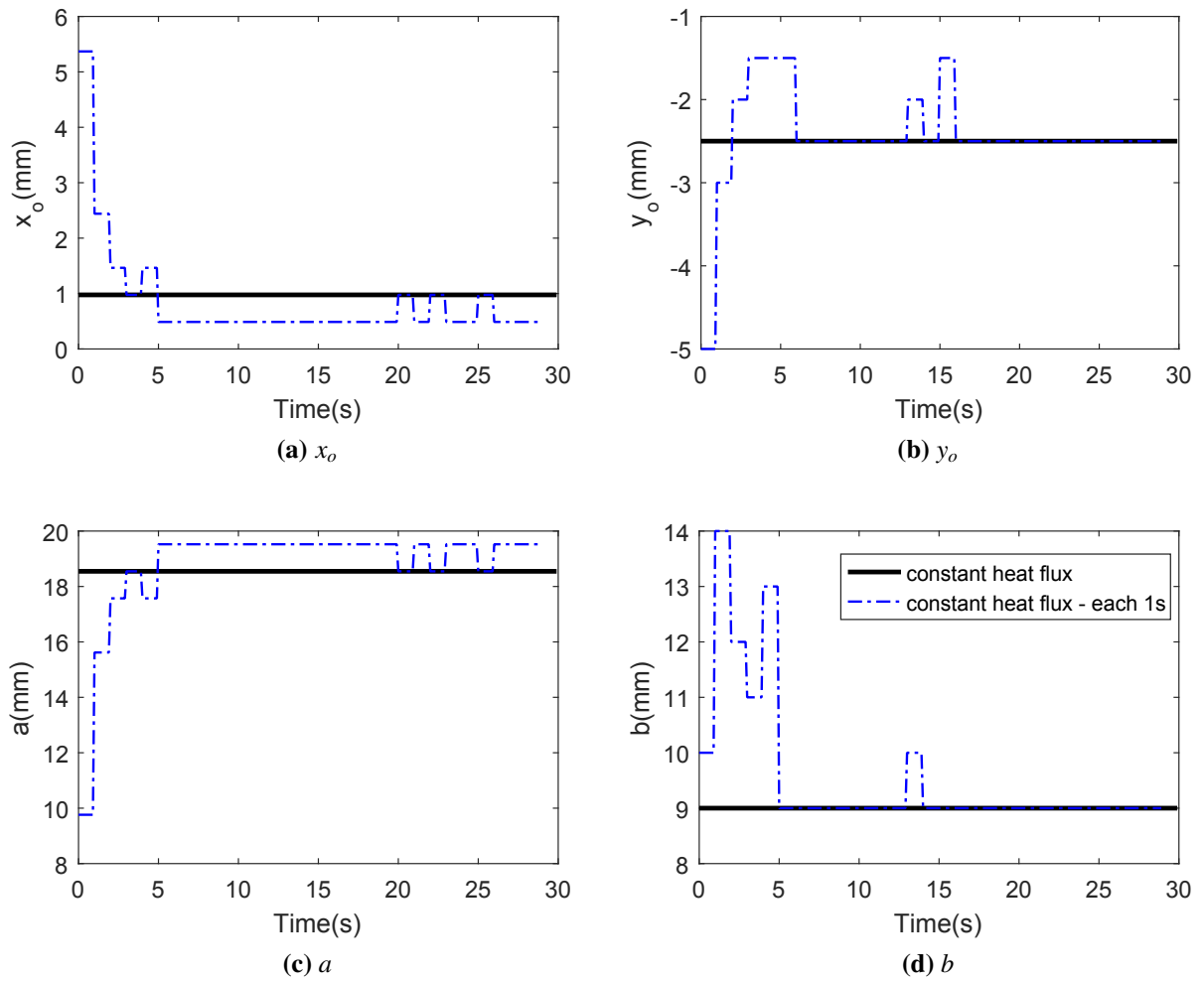


Figure 12: Temporal evolution of identified parameters (x_o , y_o , a , b) in the case of constant heat flux for each second in comparison with the case of constant heat flux over the test

2.4. Numerical model for unstable modes calculation

The finite element model for stability analysis of this pin-on-disc is developed and validated in [35]. Material behaviors of the disc, the blade and the pin support are isotropic, while the material behavior of the pin is transversal isotropic. The material data is given in Tab. 4. The contact zone is meshed with elements of 1 mm size. The mesh at the rubbing zone is compatible, meaning that there are two facing nodes of the disc and pin which have the same (x,y) coordinates at the contact zone. A fixed boundary condition is assumed for the external face of the blade and the disc (red surfaces).

Data	Disc	Pad	Thin plate	Thick plate
Young's modulus (GPa)	210	$E_x = E_y = 15.3, E_z = 5.4$	60	210
Poisson's ratio	0.3	$\nu_x = \nu_y = \nu_z = 0.15$	0.3	0.3
Density (kg/m ³)	7850	4000	2500	7850

Table 4: Material data [35]

Stability analysis aims to study the mechanism of self-excited vibrations due to frictional contact through the determination of the evolution of small perturbations around the steady sliding equilibrium. In unstable cases, some perturbations tend to diverge, which can lead to self-sustained vibrations. Such an analysis is based on a linearization of the non-linear equations around the equilibrium. A constrained non-symmetric eigenvalues problem is finally obtained as follows:

$$(M + M_\mu)\ddot{U} + (C + C_\mu)\dot{U} + (K + K_\mu)U = \mathbf{0} \quad (9)$$

where M and K denote the mass and stiffness matrices of the uncoupled system, C is the damping matrix associated to the viscous contact damping and U represents the corresponding displacements vector. M_μ, C_μ, K_μ are non-symmetrical matrices taking into account the effects of the friction forces. The formulation of these matrices can be found in [35, 54–56]. The resolution of a non-symmetrical eigenvalue problem Eq. (9) gives complex eigenvalues λ . Modes corresponding to eigenvalues with positive real part are unstable. The divergence rate of a mode is defined as $DvR = \text{Re}(\lambda)/\text{Im}(\lambda)$ where $\text{Re}(\lambda)$ and $\text{Im}(\lambda)$ are respectively the real and imaginary parts of eigenvalue λ . Due to the large size of this FE model (300000 DoFs), the resolution of Eq. (9) necessarily requires reduction methods. In order to reduce the computational, the enriched real coupled basis [35, 54–56], which perform well in [54] is used. This basis includes the real coupled basis enriched by the static part of the friction forces.

In [35], the influence of friction coefficient on the stability of the system was investigated. Using the algorithm developed by Lorang [55], the quasi-static equilibriums as a function of friction coefficient were first computed. Their corresponding distributions of quasi-static contact forces are presented in Fig. 13. The rubbing zone is assumed to be flat. A vertical displacement of 125 μm is applied on the red surface of the disc (Fig. 2) to obtain a resulting vertical contact force of 200 N. The stability analysis is then performed for these quasi-static equilibriums, leading to the graphs Fig. 14a and Fig. 14b respectively the frequency and the divergence rate. Two unstable modes are found with mode shape presented in Fig. 14c and d. These are the dominant axial movements with 3 or 4 nodal diameters and no nodal circle for the disc, as well as rotational movement (tilting) of the pin. These unstable cases are denoted as coupling 1 and coupling 2, respectively. For the first unstable mode, the friction coefficient range is between 0.28 and 0.38 at which the effective contact zone is large. For the second unstable mode, the friction coefficient range is between 0.62 and 0.8 corresponding to a smaller effective contact zone. The effective zone contact is smaller and more localized in the leading edge as shown in Fig. 13, due to the friction effect.

On the other hand, even with the same constant friction coefficient $\mu = 0.36$, it is also found a strong dependency between the squeal occurrence and contact geometry at the macroscopic scale. The influence of contact geometry on the occurrence of squeal is investigated by assuming that a macroscopic contact zone is rectangular, as shown in Fig. 8. By varying contact localization (position and dimensions), different contact zones with different sizes are defined. A sensitivity analysis is computed here by varying the width of the contact area. At a position (x_o, y_o) near the center of the nominal contact zone in Fig. 15, with $b = 11$ mm and $\mu = 0.36$, only the a dimension varies. The increase of the length a of the effective contact zone turns the unstable system from about 2100 Hz into 3500 Hz whereas only one unstable frequency at 3500 Hz appears in the case of flat contact surface. This result is similar to that obtained in [20]. Other results can be found in [35].

As mentioned by many authors (cf. [7], for instance), the complex eigenvalue problem may overestimate or underestimate the number of unstable modes. Transient analysis, which allows for the introduction of nonlinearities related to the frictional interface evolution can achieve stability analysis. However, for a large number of simulations, transient analysis proves to be very expensive on computational time. Moreover, results of transient analysis done by the authors using the θ - modified time integration scheme [57] fit with those of stability analysis.

The above numerical results showed that the same unstable frequencies could be found by modifying friction coefficient as well as contact localization. In the following section, this method is applied to friction tests. An

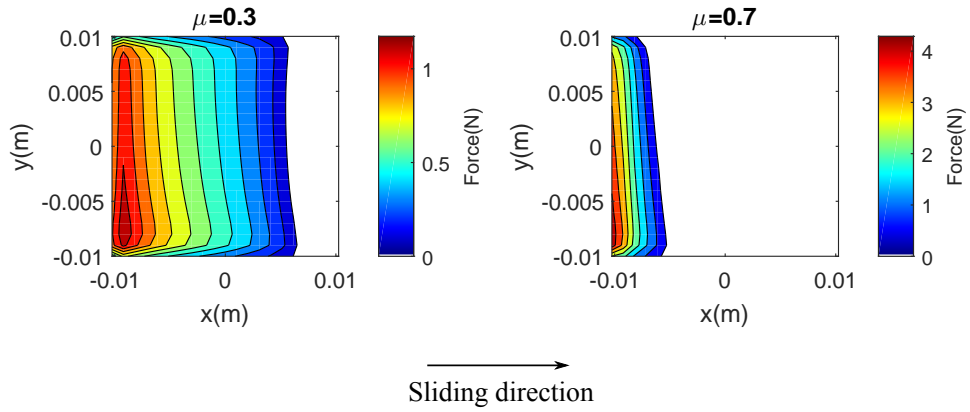


Figure 13: Distribution of contact forces on the contact area as a function of friction coefficient [35]

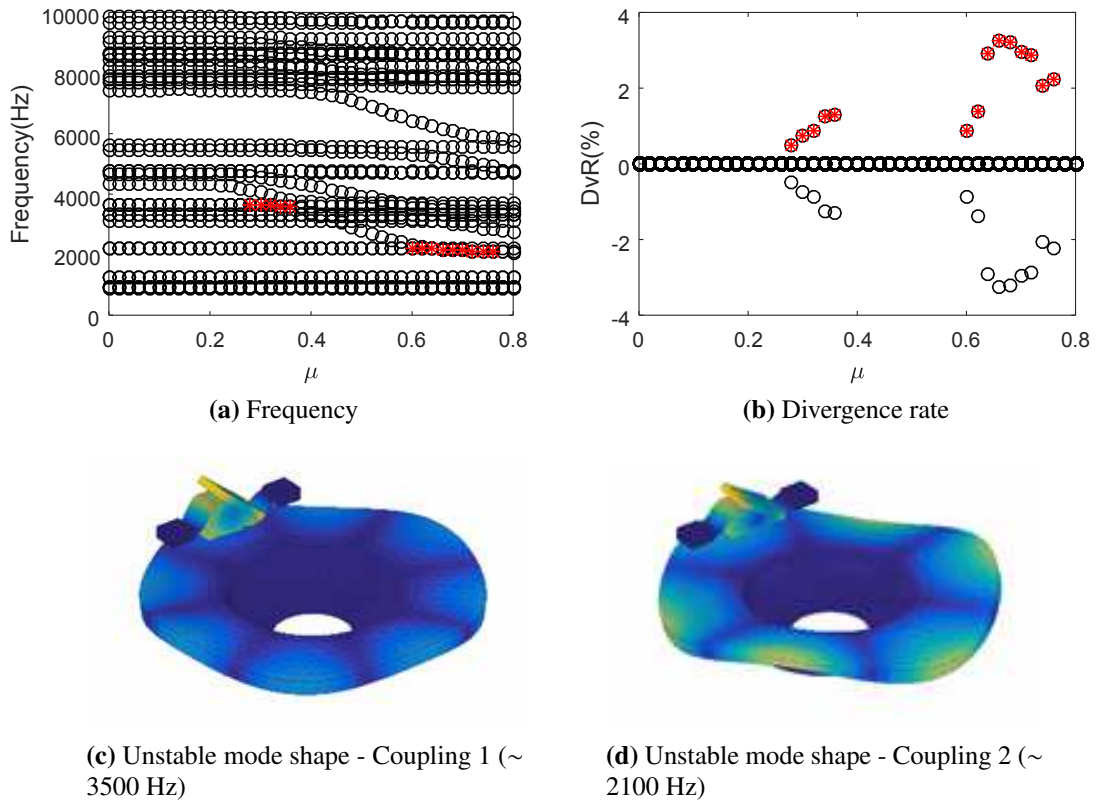


Figure 14: Stability results in the case of uniform contact as a function of friction coefficient (unstable modes frequencies in red corresponding to positive divergence rate) [35]

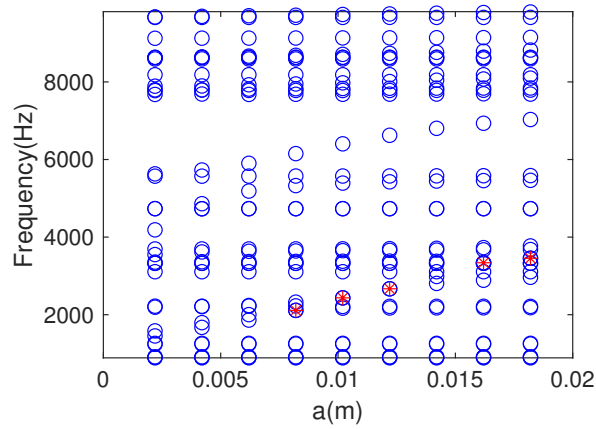


Figure 15: Evolution of complex frequencies as a function of a while x_o, y_o are fixed (close to zero) and $b = 11$ mm. Unstable modes frequencies in red corresponding to positive divergence rate.

260 investigation on the correlation between physical contact parameters (friction coefficient, contact localization) and the occurrence of squeal frequency is then performed by both experimental observations and numerical simulations.

3. Application to friction tests

3.1. Experimental observations

From the tests procedure and the post-treatment described in section 2.2, the unstable frequencies experimentally observed during tests are shown in Fig. 16a, where the marker size and color signify the duration of squeal frequencies. Two principal squeal frequencies are obtained at 3500 Hz and 2100 Hz. Squeal has not always been observed but has occurred in most tests. Looking at Fig. 16a, squeal frequency at 2100 Hz appears more often and longer after the rotation speed reaches 500 rpm. On the other hand, squeal frequency at 3500 Hz appears essentially at the rotation speed of 200 rpm. It can also be observed that no squeal is obtained when the disc rotation falls from 500 rpm to 200 rpm. Noise re-appears progressively and this phenomenon seems to be reproductive.

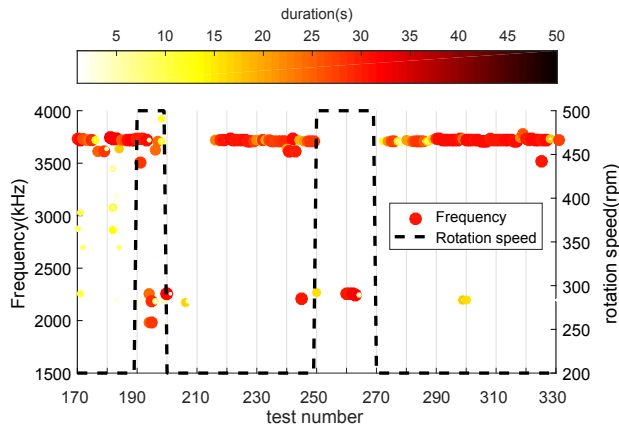
Fig. 16b shows the averaged apparent friction coefficient during these tests, which vary from 0.3 to 0.6. These coefficients have averaged values varying from 0.3 to 0.6. The measured apparent friction coefficients for these tests are almost smaller with the rotation speed of 500 rpm than those with 200 rpm. The squeal frequency at 2100 Hz occurs even with friction coefficients lower than 0.5, while the squeal frequency at 3500 Hz can be emitted with friction coefficients greater than 0.5. This is contrary to the results with the flat rubbing surface (Fig. 14a) where the frequency at 2100 Hz is obtained with high friction coefficient and at 3500 Hz with low ones. It can therefore be concluded that for these tests, the change of squeal frequencies from 3500 Hz to 2100 Hz can not be fully explained by a modification of the friction coefficient with the relative sliding speed. In terms of measured temperatures, the mean values of measured temperatures during tests are shown in Fig. 16c. Due to the higher input energy, at a rotation speed of 500 rpm, they are higher than those at a rotation speed of 200 rpm. The maximal difference between measured temperatures during this series of tests, which is defined as: $\max(T_i - T_j)$ with $i, j = 1 : 8$, increases while the rotation speed increases, as shown in Fig. 16d. The squeal frequency at 2100 Hz occurs more often while this maximal difference increases and is superior to about 20 °C. The observation leads us to consider the effect of contact localization on squeal frequencies.

3.2. Identification of load-bearing areas and consequence on instabilities

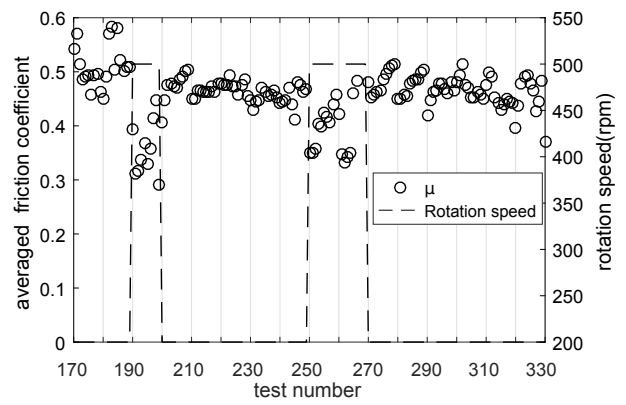
285 Firstly, to investigate the correlation between the contact localization and the occurrence of squeal, the result for the two specific tests 180 (squeal at 3.6 kHz) and 198 (squeal at 2.1 kHz) is presented. Then, for the evolution of the contact zone during tests and its consequence on instabilities, the result of stability analysis for a series of tests 170-330 is then investigated. The settings for these friction tests are presented in section 2.2.

3.2.1. Tests 180 and 198

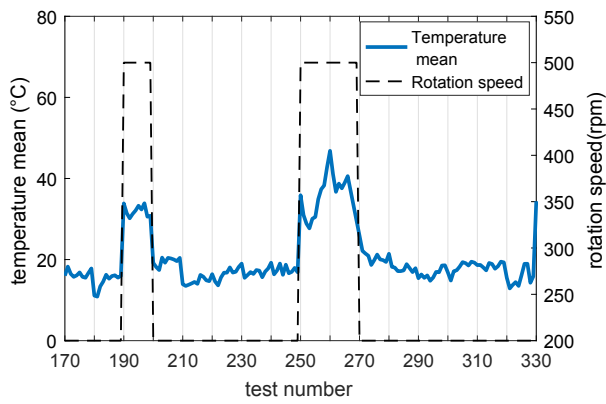
290 For example, measured temperatures by thermocouples for test 198 are presented in Fig. 17a. Compared with those for test 180 Fig. 9a, measured temperatures for test 198 are higher than for test 180 because of higher energy dissipated. This energy is related to the power of friction force, which is defined as the product of friction force and sliding velocity. It takes a value of 200 W and 500 W for tests 180 and 198, respectively. The difference between measured temperatures in thermocouples for test 198 is greater than for test 180, meaning that the contact zone is more localized. The heat flux areas identified with the inverse method previously described for these tests are presented in



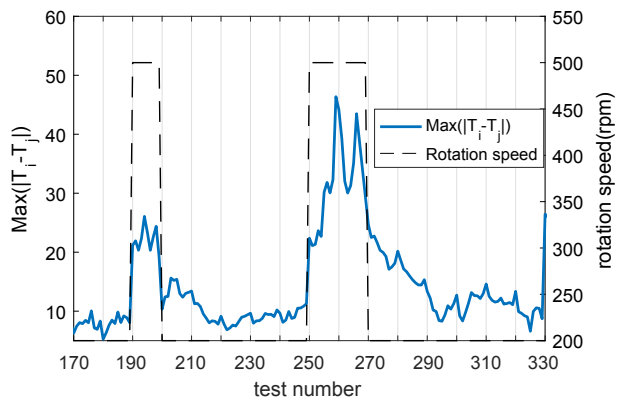
(a) squeal frequencies



(b) averaged apparent friction coefficient μ



(c) mean value of measured temperatures



(d) maximal difference between measured temperatures

Figure 16: Experimental observations during tests: Identified squeal frequencies (a), averaged apparent friction coefficient (b), value of measured temperatures (c) and maximal difference between measured temperatures (d).

Fig. 17b and Fig. 10. The identified load-bearing area for test 198 is more localized than for test 180. Physically, this higher contact localization for test 198 than for test 180 can be explained by the fact that when the greater energy dissipated in the pin, the pin is more heated. As a result of thermal dilatation, the pin shape becomes curved and the contact zone more localized. During sequences at high speed (including 198), heating is around 25°C compared to 10°C for sequences at low speed (including 180), leading to higher thermal strains and a global more deformed pin. As the natural deformation of the pin submitted to temperature gives a curvature of the surface, as described in Fig. 18, it is amplified with temperature with higher localization and more localized towards the center. Of course, this contact situation changes with wear accumulation, but that is reduced here due to the low amount of dissipated energy. A complementary influence of temperature is the effect on material properties, which could affect the dynamic behavior, especially the elastic modulus. In the present tests, heating does not exceed several dozen degrees which do not lead to any variation in the properties of this type of material, neither mechanical nor thermal as described by Mann *et al.* [58] who studied in detail the influence of temperature on these sintered type materials.

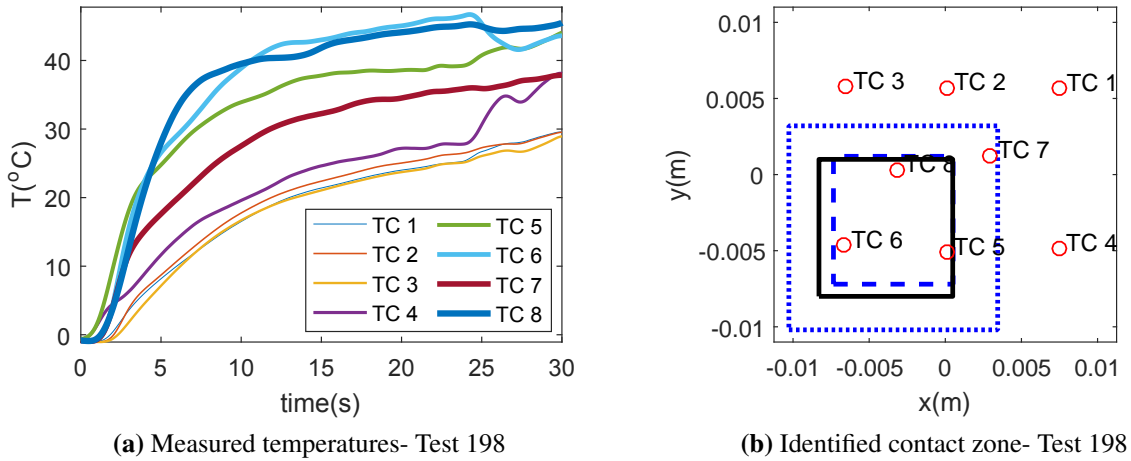


Figure 17: Measured temperatures (a) and identified contact zone (b) for test 198 (Optimal identified contact zone (black line) and 5%g_T- zones zones situated between two blue rectangles.)

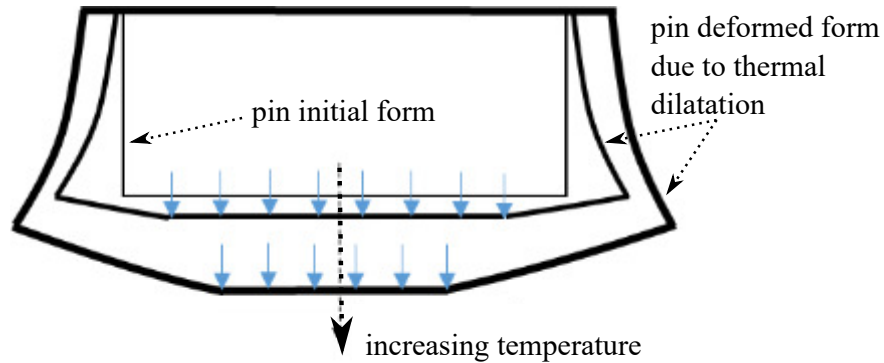


Figure 18: Illustration of the pin deformation due to thermal dilatation

Using the model presented in section 2.4, stability analysis is performed with the identified load-bearing areas and various friction coefficients. For test 180, the mechanical system is unstable around 3500 Hz with the identified load-bearing area as shown in Fig. 19a and b. For test 198, coupling 2 around 2100 Hz is found with the identified load-bearing area as shown in Fig. 19c and d. This result is consistent with experimental observation in Fig. 16 where the dominant squeal frequency is about 3700 Hz for test 180 and about 2100 Hz for test 198. For the measured friction coefficients $\mu = 0.45$ (Fig. 16c), stability analysis with the identified contact zone do not give instabilities for test 180 ($\mu_{critical} = 0.54$ in Fig. 19a) but instabilities are obtained with 5%g_T- zones as shown in Fig. 20. This means that the result of stability analysis is sensible with contact dimensions and may under-estimate instabilities. Thus, it is necessary to take into account nearby contact zones.

These results show that the squeal frequency depends on the load-bearing area during these tests. In order to investigate the influence of load-bearing area evolution on the squeal frequency variation, the results for the series of test (170-330) are then presented in the following section.

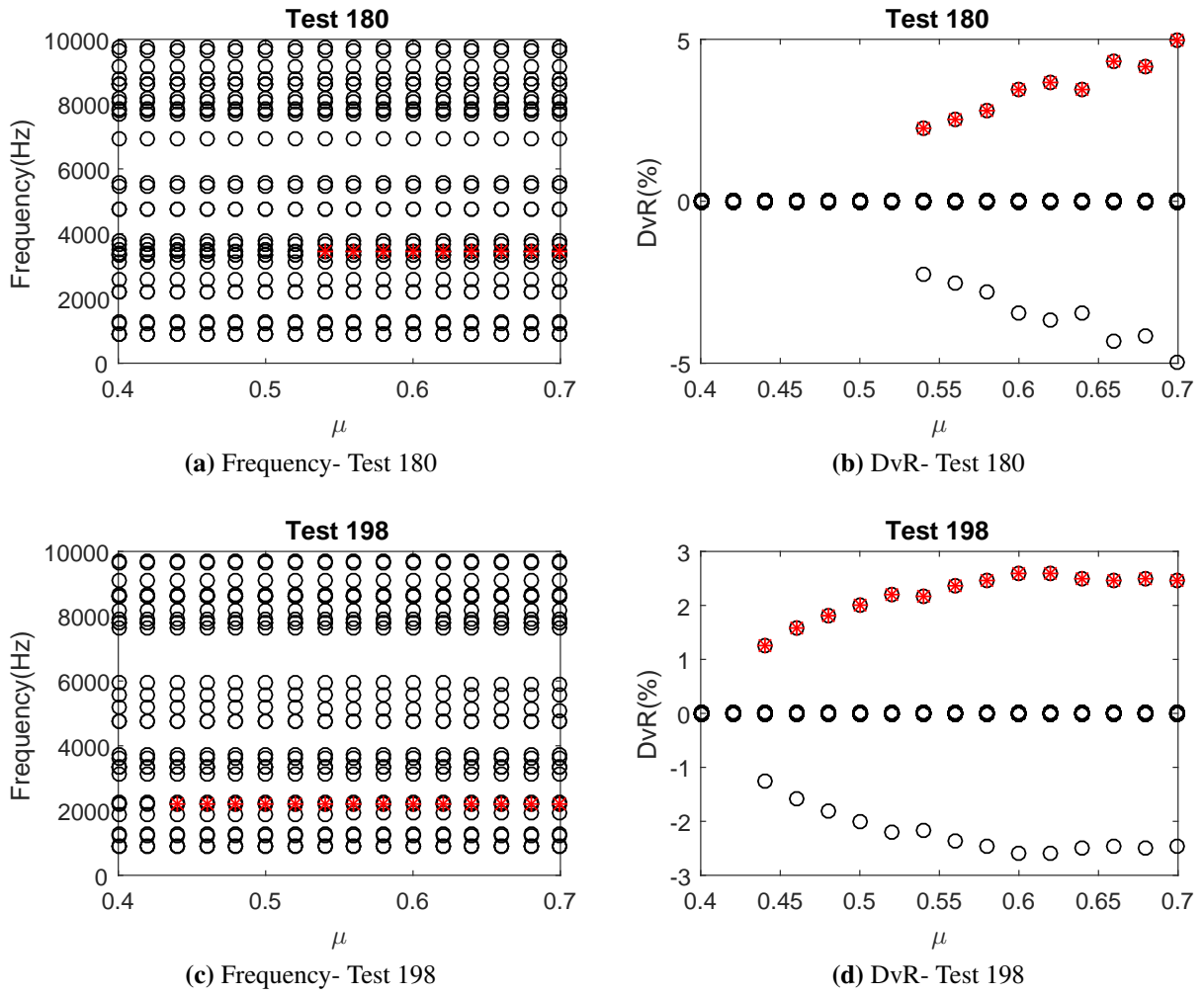


Figure 19: Stability analysis result for tests 180 and 198 with the identified "optimal" contact zone (unstable modes frequencies in red corresponding to positive divergence rate)

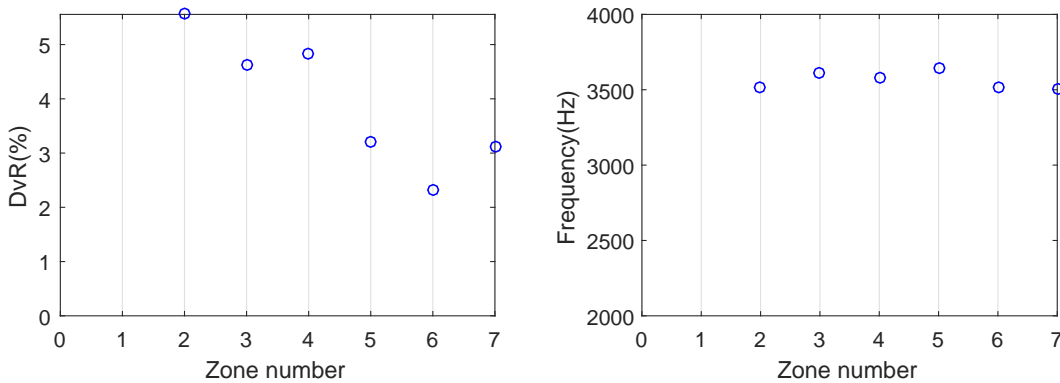


Figure 20: Stability analysis result for test 180 with the measured friction coefficient and for the various identified zones (Zone number =1: identified "optimal" contact zone, zone number=2:7 : 5% g_T - zones (blue line)) in Fig. 17.

3.2.2. Series of tests (170-330)

Fig. 21 shows the significant variation of contact parameters (x_o, y_o, a, b) of the identified load-bearing areas during successive tests (170-330). In terms of contact location, the center position x_o of the contact zone strongly evolves with the test sequence during these tests, essentially varying between the center $x_o = 0$ and the trailing edge of the rubbing surface. On the other hand, y_o remains more stable (Fig. 21a). In terms of contact dimensions (Fig. 21b), in the end of the first increase of the rotation speed (tests 190-199) and during the second increase of the rotation speed (tests 250-270), the dimension along the sliding direction a decreases. After a certain number of tests, while the rotation speed is re-established at 200 rpm (after test 290), a slightly increasing tendency of a is observed. This slight increase of a can be related to the more slowly decrease of the maximal difference between measured temperatures after the second change of rotation speed (tests after test 270), as shown in Fig. 16d. The dimension along the radial direction b increase significantly during the second increase of the rotation speed.

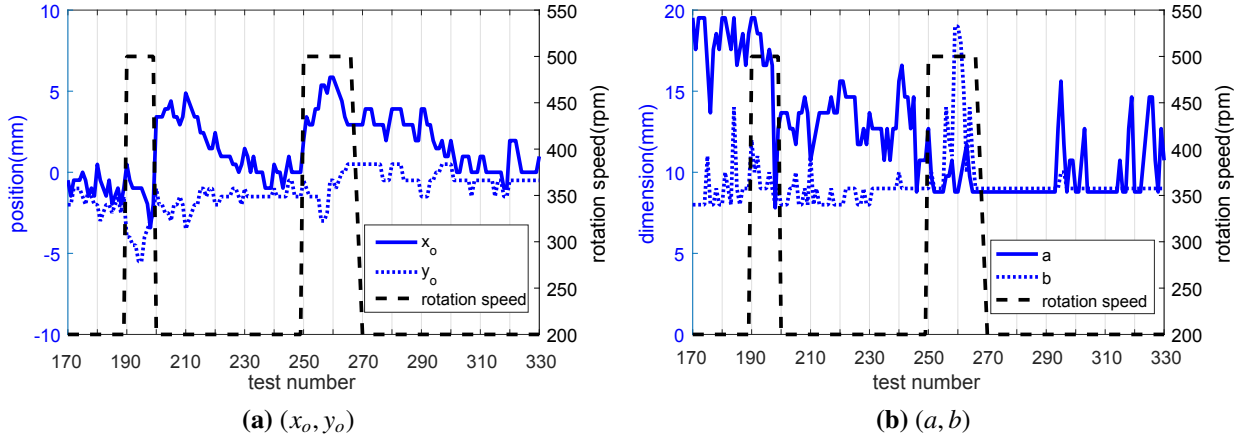


Figure 21: Results obtained by for series of tests (170-330): Center position (x_o, y_o) and b: dimensions (a, b) of the identified contact area for tests 170-330

Looking at these figures in Fig. 21, there is no clear and direct relationship between the evolution of these positions and dimensions of identified load-bearing areas with the variation of squeal frequencies. In the following, a stability analysis is then performed with the identified bearing areas. Fig. 22 shows stability analysis results obtained with the identified zone and nearby contact zones (5% g_T - zones) for the measured friction coefficients (Fig. 16c). Frequency variations from around 3500 Hz to 2100 Hz appear at the end of the first rotation speed increase or the beginning of the second rotation speed increase. This change of instabilities can be explained by the significant change of rotation speed leading to the change of contact localization at the macroscopic scale due to the thermal effect. During the second rotation speed increase, the temperature is higher, and the radial dimension b increases significantly with an increase of center position x_o (Fig. 21), which could agree with an absence of instability at around 2100 Hz. The temperatures maximal difference (Fig. 16d) takes more time to decrease during the second variation of rotation speed as same as the value of center position x_o to return close to the center of the rubbing surface together with the slight increase of the dimension along the sliding direction a (Fig. 21). These observations could agree with rather "silent" phases after the second rotation speed increase. Coupling 1 at around 3500 Hz then appears more slowly than that observed experimentally (Fig. 16a).

Recently, Sinou et al. [16] experimentally demonstrated the effects of temperature increase on the modal behavior of the brake disc, leading to the decrease of squeal frequency. The simulation results [14] also showed that instability of the disc brake is sensitive to the material properties variations of the disc brake components such as Young's modulus. In this work, with the materials used, heating is reduced, and material properties are not affected. However, the results show that contact localization always varies during friction tests. This variation greatly affects the dynamic behavior of the mechanical system in terms of squeal frequencies. Consequently, it can be concluded that the occurrence of squeal depends not only on friction coefficient, the modification of the modal behavior of the brake disc due to the thermal effect, but also on contact localization. Thus, numerical models need to consider this variation of contact localization for unstable modes calculation or quantifying transient friction-induced vibrations. It is considered here that the variation of the location affects the dynamic response without changing the properties of the contact interface, which is considered perfect. This is a point of improvement to be considered since tribological evolution potentially leads to variations in local properties that deserve to be understood, which is a perspective of this work.

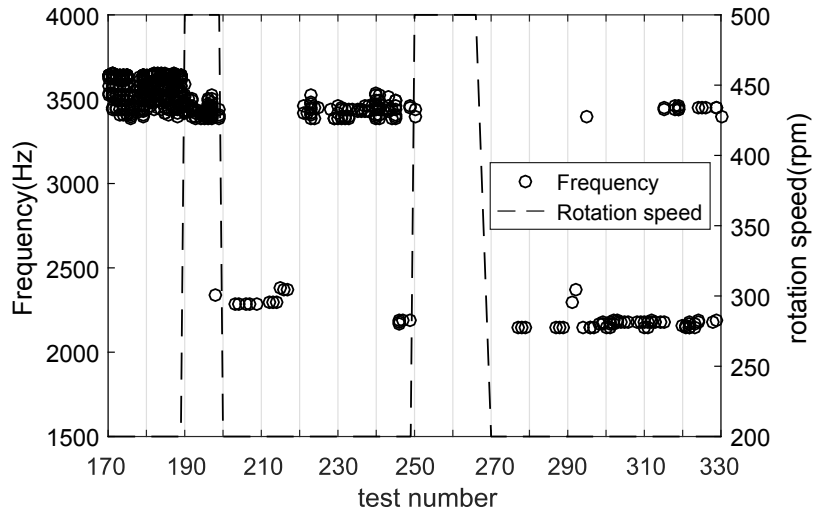


Figure 22: Stability analysis results for the series of tests 170-330 with the identified "optimal" contact zone and $5\%g_T$ - zones

3.3. Discussion

Although there is a similarity between the results and the experimental observations for the first rotation speed increase, these numerical results do not fit perfectly with the experimental observations after the second rotation speed increase. There are several possible reasons for this. First, due to the limited number of thermocouples, there is a sensibility on the identification of load-bearing areas. There exist potential solutions which give the difference between measured and numerical temperatures close to that given by the "optimal" solution. This sensibility can affect the result of stability analysis. For example: for tests (300-310), as shown in Fig. 22, the identified zone and nearby contact zones ($5\%g_T$ - zones) do not give instability at 3500 Hz, which can be obtained with $10\%g_T$ - zones, as shown in Fig. 23. Moreover, Fig. 23 also shows that the unstable frequency at 3500 Hz appears more with ($10\%g_T$ - zones) than with ($5\%g_T$ - zones). To reduce this sensibility (number of potential solutions to the inverse problem), more information needs to be added. The increase in the number of thermocouples could be a solution.

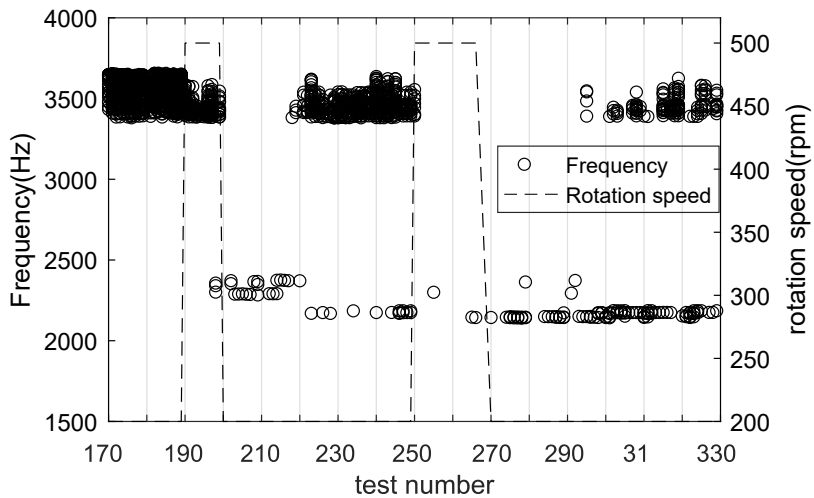


Figure 23: Stability analysis results for the series of tests 170-330 with the identified "optimal" contact zone and $10\%g_T$ - zones

Secondly, assumptions of a rectangular zone with uniform flux together with perfect contact and uniform friction coefficient do not allow to consider contact distribution at smaller scales (roughness, thirdbody, plateaus), which also has a strong impact on the stability of mechanical system [35]. Considering that brake squeal is a multiphysics-multiscale phenomenon depending on several parameters, certain unstable frequencies obtained numerically may not be activated experimentally and vice versa. Nevertheless, if one considers that the macroscopic contact zone corresponds well to the zones of flux generation, the four parameters (x_o, y_o, a, b) that define the macroscopic contact zone

375 could be "key parameters" for monitoring squeal (frequencies and occurrences). These parameters can be estimated thanks to the measurements of thermocouples and inverse calculation. This means that in the potential application of this work, monitoring the effective contact area dynamically during braking loads is an important parameter to consider for squeal occurrences and frequencies. This monitoring is difficult experimentally as it requires multi-point in-situ instrumentation such as the thermocouples used here, but it can also be addressed by numerical thermomechanical modeling. These contact localization parameters are not the only influential ones. They are major in the experiments conducted here as the temperature as far as the tribological mechanisms are limited due to reduced dissipated energy. For higher loads, the effects of variations in material and contact interface properties (surface condition, tribological mechanisms, etc.) must be added.

4. Conclusions

385 The aim of this paper is to consider the effect of rubbing contact localization on squeal. A pin-on-disc system with materials (disc and pin) from braking application has been used. Monitoring of the contact surface is carried out with thermal tracking of the friction body through thermocouples. An inverse method has been developed allowing for the approximation of macroscopic load-bearing zone from the measured temperatures inside the pin. This method involves finding uniform distribution flux on a zone with dimensions (a, b) and location (x_o, y_o) which minimize the difference between measured and numerical temperatures. It gives the location and dimensions of the contact area as well as contact heat flux intensity. Complex modal analysis of the system is performed with the identified contact zone in order to determine if the system is unstable. Results are compared with the occurrence of squeal. In operando tracking of the rubbing surface is the main novelty of this work.

Investigations along a series of tests showed that contact localization at macroscopic scale changes during friction tests. This variation can result from thermal dilatation, leading to contact concentration when temperature increases and tribological mechanisms as wear accumulate during braking sequences. The main result is obtained by comparing the macroscopic load-bearing surface variation with squeal occurrence and corresponding frequencies. It is shown that there is a correlation between these two results, and the unstable frequencies resulting from contact area variation globally match with squeal events. This is a significant result showing a strong dependency between the squeal frequencies and contact localization at the macroscopic scale. This parameter has to be considered in future studies of squeal events. This contact localization effect could be isolated thanks to tests conditions in which other phenomena such as the variation of material properties could be neutralized (limited heating, material not very sensitive in the temperature range used). It would be interesting to extend this study and to cross-reference the parameters influencing higher levels of solicitations. The results show deviations in prediction after the high rotation speed sequences (with some deviations during the silent phases or on the predicted frequencies). This can be explained by surface modifications induced by higher energy dissipation (debris ejection, variations in surface and third body states), which require considering other parameters than the evolution of the macroscopic contact surface. This is in line with the literature on the influence of the surface state on squealing and constitutes a perspective of this work. For that evolution process of thermomechanical and tribological effects on contact localization also has to be introduced.

410 It appears from this work that, given the complexity of predicting squeal, a parameter such as the variation of the effective contact area on a macroscopic scale is a key parameter. Further studies on more complex systems and situations should allow us to extend this result and to locate this key parameter among those already identified in the literature (material and surface state).

Acknowledgement

415 The present research work has been supported by the ELSAT2020 project co-financed by the European Union with the European Regional Development Fund, the French State and the Hauts de France Region Council. The authors gratefully acknowledge the support of these institutions

References

- [1] P. Dufrénoy, G. Bodovillé, G. Degallaix, Damage mechanisms and thermomechanical loading of brake discs, in: European structural integrity society, Vol. 29, Elsevier, 2002, pp. 167–176.
- [2] K. Lee, J. Barber, An experimental investigation of frictionally-excited thermoelastic instability in automotive disk brakes under a drag brake application (1994).
- [3] H. Kasem, S. Bonnamy, B. Rousseau, H. Estrade-Szwarckopf, Y. Berthier, P. Jacquemard, Interdependence between wear process, size of detached particles and CO₂ production during carbon/carbon composite friction, *Wear* 263 (7-12) (2007) 1220–1229.
- 425 [4] W. Österle, I. Dörfel, C. Prietzel, H. Rooch, A.-L. Cristol-Bulthé, G. Degallaix, Y. Desplanques, A comprehensive microscopic study of third body formation at the interface between a brake pad and brake disc during the final stage of a pin-on-disc test, *Wear* 267 (5-8) (2009) 781–788.
- [5] T. Grigoratos, G. Martini, Brake wear particle emissions: a review, *Environmental Science and Pollution Research* 22 (4) (2015) 2491–2504.
- [6] F. Massi, Y. Berthier, L. Baillet, Contact surface topography and system dynamics of brake squeal, *Wear* 265 (11-12) (2008) 1784–1792.
- 430 [7] J.-J. Sinou, Transient non-linear dynamic analysis of automotive disc brake squeal-on the need to consider both stability and non-linear analysis, *Mechanics Research Communications* 37 (2010) 96–105.

- [8] R. Jarvis, B. Mills, Vibrations induced by dry friction, proceedings of the Institution of mechanical Engineers 178 (1) (1963) 847–857.
- [9] P. Chambrette, L. Jezequel, Stability of a beam rubbed against a rotating disc, European journal of mechanics. A. Solids 11 (1992) 107–138.
- [10] N. Hoffmann, M. Fischer, R. Allgaier, L. Gaul, A minimal model for studying properties of the mode-coupling type instability in friction induced oscillations, Mechanics Research Communications 29 (2002) 197–205.
- 435 [11] C. Gao, D. Kuhlmann-Wilsdorf, D. D. Makel, Fundamentals of stick-slip, Wear 162 (1993) 1139–1149.
- [12] C. Gao, D. Kuhlmann-Wilsdorf, D. D. Makel, The dynamic analysis of stick-slip motion, Wear 173 (1-2) (1994) 1–12.
- [13] E. Denimal, J.-J. Sinou, S. Nacivet, Influence of structural modifications of automotive brake systems for squeal events with kriging meta-modelling method, Journal of Sound and Vibration 463 (2019) 114938.
- [14] A. Belhocine, N. M. Ghazaly, Effects of material properties on generation of brake squeal noise using finite element method, Latin American Journal of Solids and Structures 12 (2015) 1432–1447.
- 440 [15] R. Ibrahim, Friction-induced noise and related problems in automotive brakes, Recent Research Developments in Sound and Vibration 1 (2002).
- [16] J. Sinou, S. Besset, D. Lenoir, Some unexpected thermal effects on squeal events observed on the experimental bench five@ ecl, Mechanical Systems and Signal Processing 160 (2021) 107867.
- 445 [17] M. T. Junior, S. N. Gerges, R. Jordan, Analysis of brake squeal noise using the finite element method: a parametric study, Applied Acoustics 69 (2) (2008) 147–162.
- [18] M. Eriksson, A. Lundqvist, S. Jacobson, A study of the influence of humidity on the friction and squeal generation of automotive brake pads, Proceedings of the Institution of Mechanical Engineers, Part D: Journal of Automobile Engineering 215 (3) (2001) 329–342.
- [19] F. Bergman, M. Eriksson, S. Jacobson, The effect of reduced contact area on the occurrence of disc brake squeals for an automotive brake pad, Proceedings of the Institution of Mechanical Engineers, Part D: Journal of Automobile Engineering 214 (5) (2000) 561–568.
- 450 [20] M. Duboc, V. Magnier, J.-F. Brunel, P. Dufrénoy, Experimental set-up and the associated model for squeal analysis, Mechanics & Industry 21 (2) (2020) 204.
- [21] Z. Xiang, W. Chen, J. Mo, Q. Liu, Z. Fan, Z. Zhou, The effects of the friction block shape on the tribological and dynamical behaviours of high-speed train brakes, International Journal of Mechanical Sciences 194 (2021) 106184.
- 455 [22] M. Eriksson, S. Jacobson, Friction behaviour and squeal generation of disc brakes at low speeds, Proceedings of the Institution of Mechanical Engineers, Part D: Journal of Automobile Engineering 215 (12) (2001) 1245–1256.
- [23] E. Davin, A.-L. Cristol, J.-F. Brunel, Y. Desplanques, Wear mechanisms alteration at braking interface through atmosphere modification, Wear 426 (2019) 1094–1101.
- [24] H. Hetzler, K. Willner, On the influence of contact tribology on brake squeal, Tribology International 46 (1) (2012) 237–246.
- 460 [25] M. Eriksson, J. Lord, S. Jacobson, Wear and contact conditions of brake pads: dynamical in situ studies of pad on glass, Wear 249 (3-4) (2001) 272–278.
- [26] Y. Desplanques, G. Degallaix, Interactions between third-body flows and localisation phenomena during railway high-energy stop braking, SAE International Journal of Passenger Cars-Mechanical Systems 1 (2008-01-2583) (2008) 1267–1275.
- [27] Y. Desplanques, G. Degallaix, Genesis of the third-body at the pad-disc interface: case study of sintered metal matrix composite lining material, SAE International Journal of Materials and Manufacturing 2 (2) (2010) 25–32.
- 465 [28] S. Lee, H. Jang, Effect of plateau distribution on friction instability of brake friction materials, Wear 400 (2018) 1–9.
- [29] N. Singla, J.-F. Brunel, A. Mège-Revil, H. Kasem, Y. Desplanques, Experiment to investigate the relationship between the third-body layer and the occurrence of squeals in dry sliding contact, Tribology Letters 68 (1) (2020) 4.
- [30] Z. Xiang, J. Mo, H. Ouyang, F. Massi, B. Tang, Z. Zhou, Contact behaviour and vibrational response of a high-speed train brake friction block, Tribology International 152 (2020) 106540.
- 470 [31] A. Heussaff, L. Dubar, T. Tison, M. Watremez, R. F. Nunes, A methodology for the modelling of the variability of brake lining surfaces, Wear 289 (2012) 145–159.
- [32] D. Naidoo Ramasami, Influence of friction material & test sequence on disc brake squeal, Ph.D. thesis, Lille 1 (2014).
- [33] T. Tison, A. Heussaff, F. Massa, I. Turpin, R. Nunes, Improvement in the predictivity of squeal simulations: Uncertainty and robustness, Journal of Sound and Vibration 333 (15) (2014) 3394–3412.
- 475 [34] A. Belhocine, A. R. Abu Bakar, M. Bouchetara, Thermal and structural analysis of disc brake assembly during single stop braking event, Australian Journal of Mechanical Engineering 14 (1) (2016) 26–38.
- [35] V.-V. Lai, I. Paszkiewicz, J.-F. Brunel, P. Dufrénoy, Multi-scale contact localization and dynamic instability related to brake squeal, Lubricants 8 (4) (2020) 43.
- 480 [36] M. Stender, M. Tiedemann, D. Spieler, D. Schoepflin, N. Hoffmann, S. Oberst, Deep learning for brake squeal: Brake noise detection, characterization and prediction, Mechanical Systems and Signal Processing 149 107181.
- [37] M. Pau, B. Leban, A. Baldi, Experimental analysis of contact for the indentation of a flat rounded punch, International journal of solids and structures 43 (25-26) (2006) 7959–7965.
- [38] A. R. AbuBakar, H. Ouyang, Wear prediction of friction material and brake squeal using the finite element method, Wear 264 (11-12) (2008) 1069–1076.
- 485 [39] A. Sellami, M. Kchaou, R. Elleuch, Y. Desplanques, Thermal analysis of pad-on-disc contact under tribological solicitations: a coupled numerical–experimental approach to identify surface temperatures and flow partition coefficient, Heat and Mass Transfer 52 (9) (2016) 1923–1934.
- [40] O. M. Alifanov, Inverse heat transfer problems, Springer Science & Business Media, 2012.
- 490 [41] Z. Guo, J. Zou, Y. Chen, K. Xu, T. Lu, Online monitoring of wall temperature fluctuations of horizontal mixing t-junction pipe, Applied Thermal Engineering 127 (2017) 580–591.
- [42] C.-H. Huang, C.-C. Tsai, An inverse heat conduction problem of estimating boundary fluxes in an irregular domain with conjugate gradient method, Heat and Mass Transfer 34 (1) (1998) 47–54.
- [43] J. V. Beck, B. Blackwell, C. R. S. Clair Jr, Inverse heat conduction: Ill-posed problems, James Beck, 1985.
- 495 [44] D. Méresse, S. Harmand, M. Siroux, M. Watremez, L. Dubar, Experimental disc heat flux identification on a reduced scale braking system using the inverse heat conduction method, Applied Thermal Engineering 48 (2012) 202–210.
- [45] N. Tian, J. Sun, W. Xu, C.-H. Lai, Estimation of unknown heat source function in inverse heat conduction problems using quantum-behaved particle swarm optimization, International journal of heat and mass transfer 54 (17-18) (2011) 4110–4116.
- [46] A. Haji-Sheikh, F. Buckingham, Multidimensional inverse heat conduction using the monte carlo method (1993).
- 500 [47] H. R. Orlande, G. S. Dulikravich, Inverse heat transfer problems and their solutions within the bayesian framework, in: ECCOMAS Special Interest Conference–Numerical Heat Transfer, Vol. 640, 2012.
- [48] H.-Y. Jang, P.-C. Tuan, T.-C. Chen, T.-S. Chen, Input estimation method combined with the finite-element scheme to solve ihcp hollow-cylinder inverse heat conduction problems, Numerical Heat Transfer, Part A: Applications 50 (3) (2006) 263–280.
- [49] W. Aquino, J. C. Bringham, Self-learning finite elements for inverse estimation of thermal constitutive models, International journal of heat and mass transfer 49 (15-16) (2006) 2466–2478.
- 505

- [50] S. Deng, Y. Hwang, Solving the temperature distribution field in nonlinear heat conduction problems using the hopfield neural network, *Numerical Heat Transfer, Part B: Fundamentals* 51 (4) (2007) 375–389.
- [51] J. Krejsa, K. Woodbury, J. Ratliff, M. Raudensky, Assessment of strategies and potential for neural networks in the inverse heat conduction problem, *Inverse Problems in Engineering* 7 (3) (1999) 197–213.
- 510 [52] X. Ling, R. G. Keanini, H. Cherukuri, A non-iterative finite element method for inverse heat conduction problems, *International Journal for Numerical Methods in Engineering* 56 (9) (2003) 1315–1334.
- [53] O. Quéméner, J.-L. Battaglia, A. Neveu, Résolution d'un problème inverse par utilisation d'un modèle réduit modal. application au frottement d'un pion sur un disque en rotation, *International journal of thermal sciences* 42 (4) (2003) 361–378.
- 515 [54] D. Brizard, O. Chiello, J.-J. Sinou, X. Lorang, Performances of some reduced bases for the stability analysis of a disc/pads system in sliding contact, *Journal of Sound and Vibration* 330 (2011) 703–720.
- [55] X. Lorang, F. Foy-Margiocchi, Q. Nguyen, P. Gautier, {TGV} disc brake squeal, *Journal of Sound and Vibration* 293 (2006) 735 – 746, proceedings of the Eighth International Workshop on Railway NoiseProceedings of the Eighth International Workshop on Railway Noise. doi:<http://dx.doi.org/10.1016/j.jsv.2005.12.006>.
- 520 [56] A. Loyer, J.-J. Sinou, O. Chiello, X. Lorang, Study of nonlinear behaviors and modal reductions for friction destabilized systems. application to an elastic layer, *Journal of Sound and Vibration* 331 (2012) 1011–1041.
- [57] M. Jean, The non-smooth contact dynamics method, *Computer methods in applied mechanics and engineering* 177 (3-4) (1999) 235–257.
- [58] R. Mann, V. Magnier, J. Brunel, P. Dufrénoy, M. Henrion, E. Guillet-Revol, Thermomechanical characterization of high-speed train braking materials to improve models: Numerical validation via a comparison with an experimental braking test, *Tribology International* 156 (2021) 106818.